CHEMISTRY OF MATERIALS
Cite This: Chem. Mater. 2019, 31, 4034−4041
Article
pubs.acs.org/cm

# Lanthanide-Complex-Loaded Polymer Nanoparticles for Background-Free Single-Particle and Live-Cell Imaging

Marcelina Cardoso Dos Santos,[†,∥] Anne Runser,[‡,∥] Hortense Bartenlian,[†] Aline M. Nonat,[§] Loïc J. Charbonnière,[§] Andrey S. Klymchenko,[‡] Niko Hildebrandt,*[,†] and Andreas Reisch*[,‡]

[†]NanoBioPhotonics (nanofret.com), Institute for Integrative Biology of the Cell (I2BC), Université Paris-Saclay, Université Paris-Sud, CNRS, CEA, 91405 Orsay Cedex, France

[‡]Laboratoire de Bioimagerie et Pathologies, CNRS UMR 7021, Université de Strasbourg, Faculté de Pharmacie, 67401 Illkirch Cedex, France

[§]Equipe de Synthèse pour l'analyse (SynPA), IPHC, UMR 7178 CNRS, Université de Strasbourg, ECPM, 25 rue Becquerel, 67087 Strasbourg Cedex, France

Supporting Information

**ABSTRACT:** Imaging single molecules and nanoparticles in complex biological media is highly challenging notably due to autofluorescence of cells and tissues. Lanthanides and lanthanide complexes, with their particularly long luminescence lifetimes, offer the possibility to perform time-gated imaging and thus to strongly reduce the autofluorescence background. However, their very low brightness and photon flux have limited their use in single-molecule imaging. Here, we encapsulate high amounts of Europium complexes into poly(methyl methacrylate)-based particles of 10, 20, and 30 nm size. The resulting particles contain up to 5000 copies of the complex with a quantum yield of ≥0.2, resulting in a per particle brightness of up to $4 \times 10^7$ $M^{-1}$ $cm^{-1}$. They can be imaged at the single-particle level using low illumination intensities (0.24 W $cm^{-2}$) and low acquisition times (300 ms) and internalize well into living cells, where they can be monitored through time-gated imaging at illumination conditions compatible with living specimen. These Eu-complex-loaded nanoparticles can thus be applied for highly sensitive and autofluorescence-free imaging and have the potential to become very performant probes for fast intracellular tracking of single biomolecules.

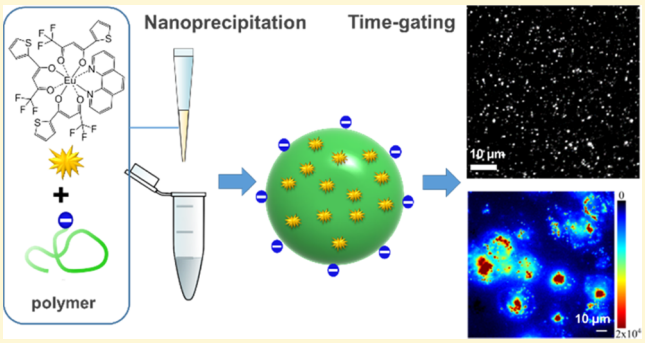


The field of luminescent nanoparticles (NPs)[1,2] for bioimaging and sensing is in constant expansion, and emerging NPs, such as semiconductor quantum dots,[3,4] upconverting NPs,[5−8] graphene or carbon dots,[9,10] lanthanide nanoparticles,[11−13] organic nanoparticles based on dyes and polymers,[14−18] and nanodiamonds,[19,20] have significantly advanced the versatility and capabilities of bioimaging applications. Detection and tracking of single NPs remain, however, challenging and often require very high illumination power and sensitive detectors to observe the particles in the presence of autofluorescence of cells and tissues.[6] Indeed, various compounds inherently present in cells or tissues, including aromatic amino acids, flavins and NAD(P)H, elastin, and porphyrins, and emitting in different wavelength regions, contribute an autofluorescence background over practically the entire visible spectrum.[21] Very bright NP probes that can be imaged while suppressing cell autofluorescence would hence offer the possibility to significantly increase the signal-to-background ratio. They would thus be valuable probes for monitoring single biomolecules with unprecedented precision directly inside living cells and thus obtain a wealth of information on biological processes at the molecular level in real time.[22,23]

Lanthanides have particularly long photoluminescence (PL) lifetimes, which offer the possibility to strongly reduce the autofluorescence background of living samples by time-gated (TG) imaging. Numerous studies have used inorganic lanthanide particles for immunodetection,[24−26] or for imaging in vitro[11,27−30] or in tissues and small animals.[31,32] However, the low photon flux of long-lived lanthanide PL (PL decay times up to milliseconds)[12] has strongly limited their use in single-particle imaging.[26,33−35] Imaging of single lanthanide particles requires near infrared irradiance power on the order of $10^3$−$10^6$ W $cm^{-2}$,[6,33,34] which can cause high phototoxicity,[36] or extremely long exposure times (30 s),[26] which are not compatible with single-molecule dynamics.

In the case of fluorescent dyes, the limits of brightness can be overcome by the so-called dye-doped or dye-loaded

Received: February 8, 2019
Revised: May 9, 2019
Published: May 29, 2019






DOI: 10.1021/acs.chemmater.9b00576
Chem. Mater. 2019, 31, 4034−4041

polymer NPs.[16,18,37−39] Encapsulation of large amounts of fluorescent dyes in these NPs allows exceeding largely the brightness of fluorescent proteins or quantum dots (up to 100-fold), while the NPs are compatible with cellular imaging.[40−42] Application of this approach to lanthanide compounds would thus offer the possibility to combine high signal with suppression of the autofluorescence background but remains largely unexplored, especially in view of high loadings, which are needed to achieve high absorbance.[43−47] Indeed, attempts to directly load high amounts of Ln complexes led to either significant quenching of the PL intensity or leakage and instability of the resulting NPs.[48,49] This was either due to insufficient retention of the complexes in the host polymer or to the formation of clusters of complexes. As a consequence, most Ln complex-loaded polymer NPs are limited with respect to their loadings and often an optimum loading of about 2 wt % was used.[45,49−53] Particularly interesting candidates for encapsulation are lanthanide complexes (chelates or cryptates), which provide much higher absorption cross sections and PL quantum yields (QYs) than those of the pure lanthanide ions and have been used in many biosensing applications.[12,54] Loading of high amounts of these bright lanthanide complexes with long PL lifetimes into small polymeric NPs has the potential to extend NP-based PL imaging to challenging biological samples (e.g., tissues) with high intrinsic autofluorescence through the use of TG. In this work, we demonstrate that single-particle and live-cell imaging of small polymer NPs (down to 10 nm) loaded with lanthanide complexes can be performed with short acquisition times and low irradiation power (Figure 1). Our proof-of-concept study demonstrates

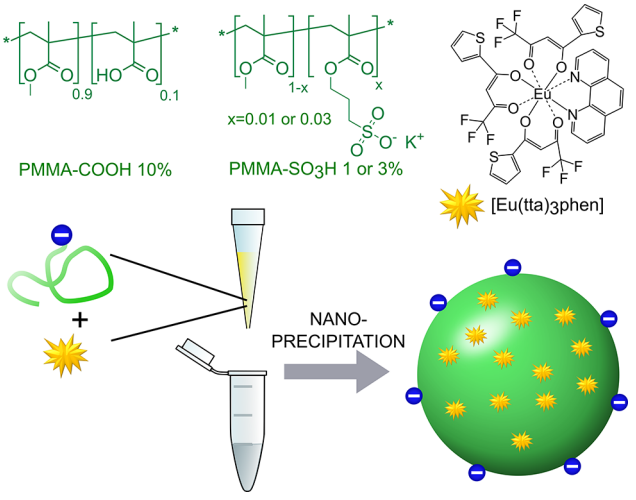


**Figure 1.** Chemical structures of the polymers and the lanthanide complex used in this study, and schematic representation of the synthesis of Europium-complex-loaded polymer NPs (ECP-NPs).

the possibility to extend lanthanide-NP imaging toward single-particle tracking and thus their potential as probes for the investigation of cellular and molecular dynamics.

## RESULTS AND DISCUSSION

Europium-complex-loaded polymer NPs (ECP-NPs) were prepared through nanoprecipitation of acetonitrile solutions containing the $Eu^{3+}$-complex and methyl methacrylate-based copolymers (PMMA) bearing sulfonate (1 and 3 mol %) or carboxylate (10 mol %) groups in water (Figure 1). The charged groups were introduced during polymerization to reduce and control the size of the particles.[55,56] We encapsulated 1−40 wt % (relative to the polymer) of $Eu(tta)_3phen$ ($Eu^{3+}$ surrounded by three [4,4,4-trifluoro-1-(2-thienyl)-1,3-butanedionate] and 1,10-phenantroline ligands)[57] inside the NPs. This resulted in three series of ECP-NPs with mean diameters, as obtained from transmission electron microscopy (TEM), of ∼30, ∼20, and ∼10 nm for PMMA-COOH 10%, PMMA-$SO_3H$ 1%, and PMMA-$SO_3H$ 3%, respectively (Figure 2). Particle sizes slightly increased with

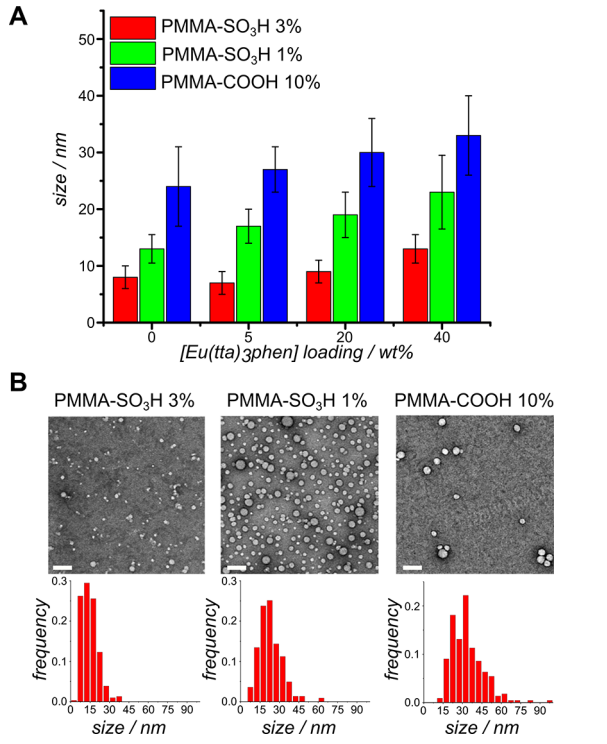


**Figure 2.** (A) Size measurements of ECP-NPs by TEM. NPs of PMMA-$SO_3H$ 1 and 3% and PMMA-COOH 10% were loaded with different amounts of $[Eu(tta)_3phen]$. Sizes are mean values over at least 200 particles; error bars correspond to width at half-maximum of the size distributions. (B) TEM images and size distribution of NPs at 40 wt % $[Eu(tta)_3phen]$ loading made from different polymers. Scale bars correspond to 100 nm. At least 100 NPs were analyzed per condition.

increasing $Eu(tta)_3phen$ loading. At the highest loading of 40 wt % $Eu(tta)_3phen$, TEM showed spherical NPs with sizes of 13, 23, and 34 nm, respectively, and relatively narrow size distributions (Figure 2B). Especially, in view of their future use as labels for intracellular imaging, small sizes are important.[56,58] The smallest ECP-NPs obtained here have sizes on the order of those of antibodies, which makes them particularly attractive as labels for single biomolecules. Encapsulation of the $Eu^{3+}$ complex was confirmed by the higher contrast of the loaded NPs in TEM (Figure S1).

We then characterized the photophysical properties of these ECP-NPs. Their absorption showed no spectral variations (compared to those for $Eu(tta)_3phen$ in organic solution) and the absorbance increased with $Eu(tta)_3phen$ loading (Figure S2). ECP-NP emission spectra clearly showed the $Eu(tta)_3phen$ characteristics with intense PL of the hypersensitive $^5D_0 \rightarrow {}^7F_2$ transition of $Eu^{3+}$ between 610 and 630 nm (Figures 3A and S2).[59] PL quantum yields (QYs) in water


DOI: 10.1021/acs.chemmater.9b00576
Chem. Mater. 2019, 31, 4034−4041

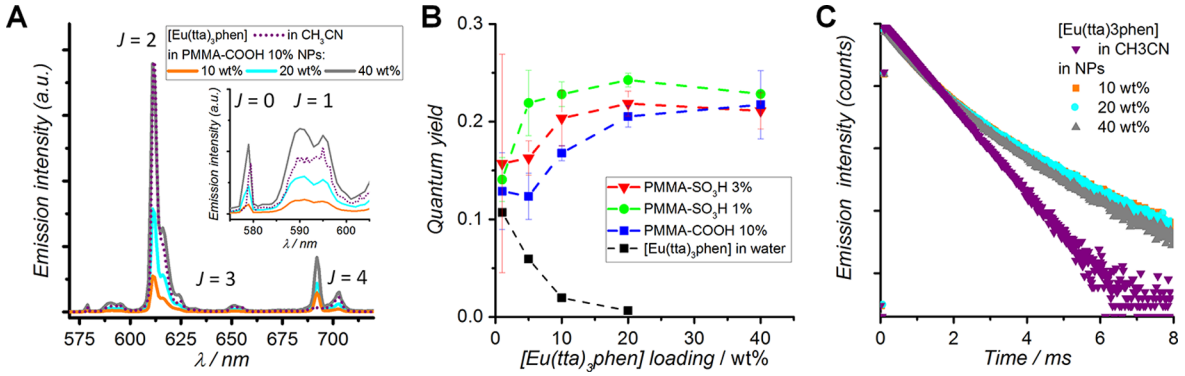


**Figure 3.** (A) Emission spectra ($\lambda_{exc}$ = 350 nm) recorded in aqueous solution for PMMA-COOH 10% NPs loaded with different amounts of [Eu(tta)$_3$phen], as well as of [Eu(tta)$_3$phen] in $CH_3CN$. Inset: Zoom on the $^5D_0 \rightarrow {}^7F_{J=0,1}$ transitions. (B) Photoluminescence quantum yields of ECP-NPs vs [Eu(tta)$_3$phen] loading. Data points correspond to mean values from three independent measurements. Error bars correspond to standard error of the mean. ([Eu(tta)$_3$phen] in water at a concentration corresponding to 40 wt % in the NPs led to the formation of sedimenting aggregates.) (C) Time-resolved emission decay profiles (rt, $\lambda_{exc}$ = 350 nm) measured for solutions of [Eu(tta)$_3$phen] in acetonitrile and of PMMA-COOH 10% NPs loaded with different amounts of [Eu(tta)$_3$phen]. Note: Log scale for emission intensity.

**Table 1. Lifetimes of [Eu(tta)$_3$phen] in Acetonitrile and of ECP-NPs in Water**[a,b]

| | $\tau_1$ | | $\tau_2$ | |
|---|---|---|---|---|
| | ms | % | ms | % |
| [Eu(tta)$_3$phen] in $CH_3CN$ | 0.625 | 100 | | |
| PMMA-COOH 10%−10% [Eu(tta)$_3$phen] | 0.524 | 50 | 1.301 | 50 |
| PMMA-COOH 10%−20% [Eu(tta)$_3$phen] | 0.524 | 50 | 1.301 | 50 |
| PMMA-COOH 10%−40% [Eu(tta)$_3$phen] | 0.553 | 65 | 1.218 | 34 |

[a]Room temperature (rt), $\lambda_{exc}$ = 350 nm. [b]Estimated errors: ±10% on lifetimes.

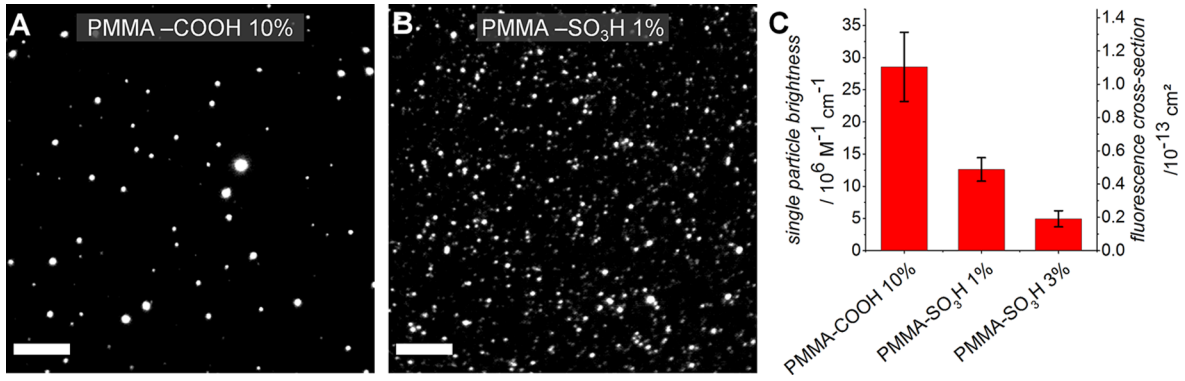


**Figure 4.** TG single-particle images of PMMA-COOH 10% (A) and PMMA-$SO_3H$ 1% (B) at 40% [Eu(tta)$_3$phen] loading. Scale bars: 10 $\mu$m. (C) Average single-particle PL brightness in $M^{-1}$ $cm^{-1}$ and their correspondence in luminescence cross section as obtained from single-particle microscopy. At least 100 particles were analyzed for each condition. Error bars correspond to SD.

increased with Eu(tta)$_3$phen loading and reached a maximum of ~0.25 at around 20 wt % (Figure 3B). QYs were highest in PMMA-$SO_3H$ 1%, followed by PMMA-$SO_3H$ 3% and PMMA-COOH 10% (Table S1). The biexponential PL decays of ECP-NPs indicated two distinct populations of Eu(tta)$_3$phen inside the NPs (Figure 3C and Table 1). The shorter decay time ($\tau_1$ = 0.54 ± 0.02 ms) was in the same range as for Eu(tta)$_3$phen in acetonitrile ($\tau$ = 0.63 ms) and therefore assigned to a population close to the surface of the NPs. The longer decay ($\tau_2$ = 1.26 ± 0.04 ms) exceeded the lifetime of Eu(tta)$_3$phen measured in solid state ($\tau$ = 0.87 ms)[60] and was therefore assigned to a population in the core of the NPs.

These results indicate an efficient encapsulation of Eu(tta)$_3$phen in the polymer NPs and a good protection of the Eu cations from water deactivation. Indeed, addition of Eu(tta)$_3$phen to water (in the absence of polymer) led to aggregation and thus a strong decrease in the absorbance together with QYs close to zero (Figure 3B). The influence of the nature of the polymer on the QY could stem from the differences in size of the resulting NPs, the number of charged groups, or their nature. No clear correlation with size was observed. At the same time, the QYs decreased with increasing fraction of charged groups on the polymer. These might hence interact with part of the complexes, as their concentrations lie in a similar range. The nature of the charged groups could also play a role, with carboxylates interacting more strongly with the complexes than sulfonates. The observed increase in QY with loading of the complex could be explained by a higher fraction of the complex encapsulated in the core of the NPs, which is characterized by a prolonged lifetime. The increase of the PL decay time upon encapsulation is of high interest for applications such as time-resolved microscopy or fluoroimmu-



DOI: 10.1021/acs.chemmater.9b00576
Chem. Mater. 2019, 31, 4034−4041

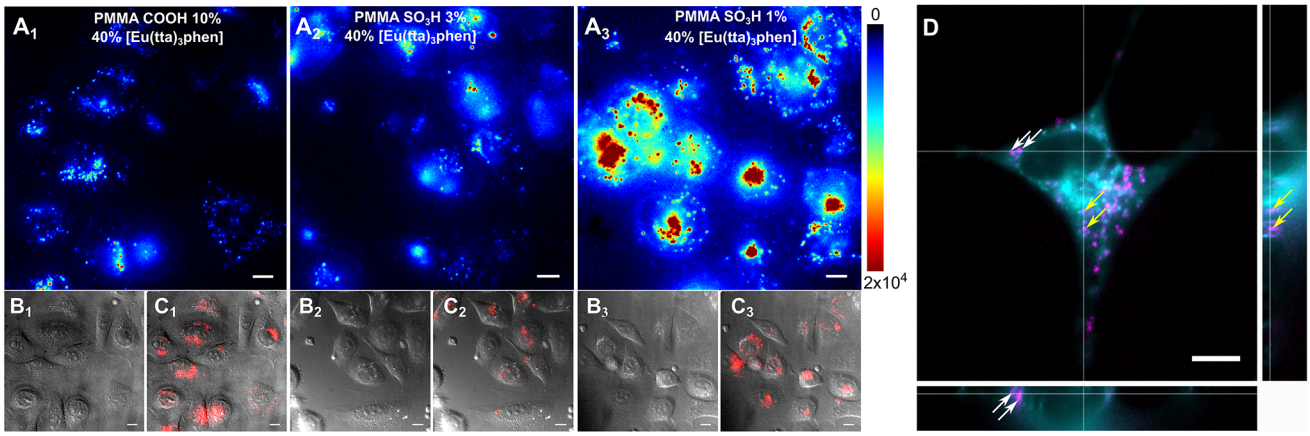


**Figure 5.** Live-cell images of HeLa cells incubated with ECP-NPs. (A) TG PL images with PMMA-COOH 10% ($A_1$), PMMA-$SO_3H$ 3% ($A_2$), and PMMA-$SO_3H$ 1% ($A_3$) NPs at 40% [$Eu(tta)_3phen$] loading. For a better comparison between the different images, the intensity scale was fixed at 0 to 2 × $10^4$ counts. (B) Differential interference contrast (DIC) images. (C) Overlay of images from A and B (ECP-NP PL is shown in red, PL intensities were normalized to the highest values in A1, A2, and A3). (D) Projections of a z-stack of images of a HeLa cell incubated with ECP-NPs (PMMA-COOH 10% at 40% [$Eu(tta)_3phen$]). ECP-NPs are shown in magenta and the cell membranes in turquoise (costained with DiD). Large image: $x/y$-optical section at 6 $\mu$m from the surface; small images are optical sections of cell along the $x$- and $y$-axis of the z-stack with a $x/z$ side view (bottom) and $y/z$ side view (right). Lines in the images indicate positions of the sections; white and yellow arrows point to ECP-NPs in endosomes/lysosomes. Scale bars in all images: 10 $\mu$m.

noassay because it allows for a more efficient autofluorescence background suppression. Interestingly, practically, no concentration quenching was observed for these complexes, at least up to 20 wt %. This results in a very high brightness of the obtained luminescent NPs: the PMMA-COOH 10% NPs of 34 nm encapsulate about 5000 complexes per particle (based on NP size for 40 wt % loading) with a QY of 21%, yielding a brightness, B, of 0.21 × 40 000 $M^{-1}$ $cm^{-1}$ × 5000 = 4.2 × $10^7$ $M^{-1}$ $cm^{-1}$ and a luminescence cross section, $\sigma$, of 1.6 × $10^{-13}$ $cm^2$ (see the Methods section for calculations). For the PMMA-$SO_3H$ 1 and 3% NPs, the corresponding brightness is 1.2 × $10^7$ and 0.34 × $10^7$ $M^{-1}$ $cm^{-1}$, respectively. These differences are first of all due to the differences in size and the resulting variation of the number of complexes per particle. Indeed, dividing the particle brightness by the particle volume gives similar values of (2100 ± 200) $M^{-1}$ $cm^{-1}$ $nm^{-3}$ for all three polymers. The brightness of our ECP-NPs thus largely exceeds that of classical molecular fluorophores (on the order of $10^5$ $M^{-1}$ $cm^{-1}$) and even that of the brightest quantum dots (e.g., 7.4. × $10^6$ $M^{-1}$ $cm^{-1}$ for QDot 625 from Invitrogen).

Taking advantage of the exceptional brightness of our ECP-NPs, we assessed their performance for single-particle imaging using both continuous illumination (for photon counting) and TG imaging. For this, very dilute solutions of the NPs were deposited on polyethylenimine (PEI)-treated glass or in poly(vinyl alcohol) (PVA) gels under conditions favoring immobilization as single particles.[40,41] The NPs could be imaged at the single-particle level in both imaging modes (Figures 4, S3, and S4): using a setup for photon counting and steady-state illumination allowed us to determine the absolute brightness of the particles as 2.9 × $10^7$, 1.2 × $10^7$, and 0.5 × $10^7$ $M^{-1}$ $cm^{-1}$, respectively, for the 40 wt % PMMA-COOH 10%, PMMA$SO_3H$ 1%, and PMMA$SO_3H$ 3% particles ($\sigma$ = 1.1, 0.48, and 0.18 × $10^{-13}$ $cm^2$, respectively). These values are in reasonable agreement with the particle brightness obtained from spectroscopic data, and in line with their size and thus the number of encapsulated complexes per particle (see the Supporting Information for details on calculations). In TG imaging (detection window from 0.01 to 0.61 ms after pulsed excitation),[61] efficient detection of single particles of all three types of ECP-NPs loaded with 40 wt % of $Eu(tta)_3phen$ was accomplished with excitation power densities as low as 0.24 W $cm^{-2}$ and an impressively short total acquisition time (for lanthanide detection) of 666 ms (Figures 4 and S3). The brightness of the particles in TG imaging also increased in the order PMMA-$SO_3H$ 3% < PMMA$SO_3H$ 1% < PMMA-COOH 10%. It should be noted that these results could be obtained on an imaging setup that used extremely low light doses in the sub $\mu$J $cm^{-2}$ range, which is several orders of magnitude lower than those used in conventional fluorescence imaging studies and thus avoids cytotoxic effects.[11] Besides being even brighter than QDs, the ECP-NPs have thus the distinct advantage that they are suitable for TG imaging down to the single-particle level, which opens the way to suppression of autofluorescence background in cellular imaging.

Encouraged by the single-particle imaging capability of the ECP-NPs, we investigated their potential for live-cell imaging. For this purpose, the NPs were incubated for 3 h with HeLa cells and TG imaging was performed with a very low excitation power density of 0.24 W $cm^{-2}$, which is compatible with biological samples and 4 orders of magnitude lower compared to conventional lanthanide-based imaging.[62] Figure 5 shows strong PL signals from endocytosed ECP-NPs, for both the sulfonate- and the carboxylate-based particles. Highest luminescence was observed for the PMMA-$SO_3H$ 1% particles followed by PMMA-$SO_3H$ 3% and PMMA-COOH 10% particles, which indicates the highest uptake efficiency for the former NPs. These differences indicate that sulfonate bearing NPs are more readily internalized than those bearing carboxylate. However, as size and NP concentration change at the same time, it is difficult to derive general relations. An acquisition time of 333 ms (0.01 ms delay, 0.6 ms gate, 100 gates/exposure), corresponding to acquisition times used in conventional imaging, was sufficient to clearly image our NPs inside cells. To better appreciate the localization of NPs inside the cells, PL and differential interference contrast (DIC) images were overlayed and the intensity scale adapted according to the PL level (Figure 5C). In addition, TG


DOI: 10.1021/acs.chemmater.9b00576
Chem. Mater. 2019, 31, 4034−4041

imaging eliminates all autofluorescence, such that the experiments could be performed in complete cell culture medium (Figure S8). The intracellular position of the ECP-NPs was studied by optical sectioning of HeLa cells in the *Z*-direction (Figure 5D, Supporting Information Movie S1), by imaging after different incubation times (Figure S9), and by costaining with LysoTracker (Figure S6). These experiments indicated that the ECP-NPs first adsorbed on the membrane and then located in endosomes or lysosomes inside the cells. To investigate intracellular brightness as a function of Eu-(tta)$_3$phen loading, cells were incubated with carboxylate polymer NPs at 40, 20, 10, and 5% doping ratios (Figure S7). At the highest loading ratio, PL intensities of the brightest points inside the cells exceeded 10 000 counts, whereas those at the lowest loading ratio still reached 1000 counts, confirming increasing luminescence intensity of the particles with increasing loading directly in the cells.

To investigate a long-term effect of NPs on live cells, we controlled cell development within 7 days for cells incubated with NPs PMMA-SO$_3$H 3% at 20% [Eu(tta)$_3$phen] loading (Figure S10A). The results showed no influence of the NPs on cell development. Furthermore, the presence of NPs was observed in cells even after 7 days postincubation (Figure S10B), even though their luminescence decreases according to cell division.

## CONCLUSIONS

ECP-NPs with diameters of 10, 20, and 30 nm and up to 40 wt % of Eu-complex loading were successfully assembled by nanoprecipitation. This corresponds to encapsulation of up to 5000 emitters per particle, thus reaching very high absorbance. The ECP-NPs showed high PL QYs in water (up to 0.26) and long PL decay times (up to 1.3 ms). High loading together with high QYs led to an exceptionally high brightness of more than $10^7$ $M^{-1}$ $cm^{-1}$. Together with their millisecond lifetimes, this allowed us to use ECP-NPs for TG imaging at the single-particle level at low laser powers and short acquisition times. ECP-NPs were spontaneously endocytosed and detected by autofluorescence-free TG imaging inside live HeLa cells in the presence of whole culture medium. Our Eu-complex-doped polymer NPs successfully demonstrated that lanthanide-based NPs can be applied for highly sensitive and autofluorescence-free imaging using a standard TG wide-field fluorescence microscope and low excitation powers. Upon suitable functionalization, they could thus be applied to label biomolecules and allow their imaging at the single-particle level with high spatial and temporal resolution, even in complex biological systems. The ECP-NPs presented here thus open a whole new field of high-precision tracking of single biomolecules at low excitation light conditions inside living cells.

## METHODS

**Materials.** Milli-Q water (Millipore) and acetonitrile (≥99.9%, Sigma-Aldrich) were used for the preparation of NPs. CELLview Petri dishes (35 × 10 mm, Greiner Bio-One, 627860), Nunclon Delta Petri dishes (35 × 12 mm, Nunc, 150318), and LabTek II (8 well, Nunc, 155409) cell culture chambers were used for cell and single NP imaging. Polyethylenimine (PEI, 408727) and poly(vinyl alcohol) (PVA, Sigma-Aldrich, 341584) were used to immobilize single NPs on the glass surface. Human cervical carcinoma (HeLa) cells were purchased from American Type Culture Collection (CCL-2). Dulbecco's modified Eagle medium (DMEM, D6546), fetal bovine serum (FBS, F0804), antibiotics (Pen Strep, P4333), L-glutamine (G7513), and trypsin−ethylenediaminetetraacetic acid (EDTA) 0.05% (59417C) for cell culture were purchased from Sigma-Aldrich. Opti-MEM I reduced serum medium (1×, Gibco, 11058-021), Hank's balanced salt solution (HBSS, Sigma-Aldrich, H6648), and fibronectin (Sigma-Aldrich, F1141) were used for cell imaging. DID probe (1,1′-dioctadecyl-3,3,3′,3′-tetramethylindodicarbocyanine, 4-chlorobenzenesulfonate salt, D7757, Molecular Probes, Invitrogen) and LysoTracker green DND-26 (ThermoFisher Scientific, L7526) were used for colocalization imaging.

**Polymer Synthesis.** Poly(methyl methacrylate)s bearing carboxylate groups at 10 mol % (PMMA-COOH 10%) and sulfonate groups at 1 or 3 mol % (PMMA-SO$_3$H 1 and 3%) were synthetized through copolymerization of methyl methacrylate (Sigma-Aldrich, M55909) with methacrylic acid (Sigma-Aldrich, 155721) or 3-sulfopropyl methacrylate potassium salt (Sigma-Aldrich, 251658), respectively, via radical polymerization at 70 °C using azobisisobutyronitrile as an initiator, and reprecipitated twice in methanol. PMMA-COOH 10%: $^1$H NMR (400 MHz, $CDCl_3$, $\delta$): 3.60 (s, 3 H), 2.2−0.5 (m, 6 H). Molecular weight by size exclusion chromatography (SEC): $M_w$ = 35 200, $M_w/M_n$ = 1.29. PMMA-SO$_3$H: $^1$H NMR (400 MHz, DMSO-$d_6$, $\delta$): 3.97 (br. s, 0.02; 0.06 H), 3.57 (s, 3 H), 2.45 (m, partial covered by the solvent peak), 2.1−0.5 (m, 6 H). % Molecular weight by SEC: 1%: $M_w$ = 51,200, $M_w/M_n$ = 1.58; 3%: $M_w$ = 106,600, $M_w/M_n$ = 1.37.

**Preparation of Nanoparticles.** Stock solutions of PMMA-COOH 10% and PMMA-SO$_3$H 1 and 3% were prepared at a concentration of 10 g $L^{-1}$ in acetonitrile. These solutions were diluted to 2 g $L^{-1}$ for PMMA-COOH 10% and PMMA-SO$_3$H 1% and 1.2 g $L^{-1}$ for PMMA-SO$_3$H 3% in acetonitrile containing different amounts of [Eu(tta)$_3$phen] (0−40 wt % relative to the polymer). Polymer solution (50 $\mu$L) was added in 450 $\mu$L of water with a micropipette under shaking at 21 °C. Then, the obtained suspension was quickly diluted 5-fold in water.

**Characterization of Nanoparticles.** *Transmission Electron Microscopy (TEM).* Nanoparticle solution (5 $\mu$L) at 40 $\mu$g $mL^{-1}$ was deposited onto carbon-coated copper−rhodium electron microscopy grids following amylamine glow discharge. They were then treated for 1 min with a 2% uranyl acetate solution for staining. The obtained grids were observed using a Philips CM120 TEM equipped with a LaB6 filament and operating at 100 kV. The acquisition of areas of interest was performed with a Peltier-cooled charge-coupled device (CCD) camera (model 794, Gatan, Pleasanton, CA). Images were analyzed using Fiji software.

*Spectroscopy.* Absorption and emission spectra of NPs were recorded on a Cary 4000 Scan ultraviolet−visible spectrophotometer (Varian) and a FluoroMax-4 spectrofluorometer (Horiba Jobin Yvon) equipped with a thermostated cell compartment, respectively. The excitation wavelength was set to 345 nm, and emission was recorded from 550 to 720 nm. QYs of the NPs were calculated using [Eu(tta)$_3$phen] in acetonitrile as a reference (QY = 0.30, see below). For [Eu(tta)$_3$phen] in acetonitrile, UV−visible absorption spectra were recorded on a Specord 205 (Analytik Jena) spectrometer, whereas steady-state emission and excitation spectra were recorded on a FLP920 spectrometer from Edinburgh Instruments working with a continuous 450W Xe lamp and a red-sensitive Hamamatsu R928 photomultiplier in a Peltier housing. All spectra were corrected for the instrumental functions. A 455 nm highpass filter was used to remove second-order artifacts. Phosphorescence lifetimes were measured on the same instrument working in a multichannel scaling mode and using a Xenon flash lamp as the excitation source. Errors on the PL lifetimes were estimated to ±10%. PL quantum yields of [Eu(tta)$_3$phen] in acetonitrile were determined independently using an absolute method (QY= 0.32) on a Horiba Jobin Yvon Fluorolog 3 spectrometer equipped with a G8 integration sphere (GMP SA, Switzerland) and by comparison with a reference sample, [TbL(H$_2$O)] in water (QY = 0.31, $\lambda_{exc}$ = 308 nm)[63], using optically diluted solutions (optical density <0.05) and yielding QY of 0.28. Estimated errors on the PL quantum yields were ±15%, and the reported value for [Eu(tta)$_3$phen] in acetonitrile (0.30) was taken as the average of both methods. The particle brightness is then obtained as follows: the number of emitters can be calculated based on the wt % of


DOI: 10.1021/acs.chemmater.9b00576
Chem. Mater. 2019, 31, 4034−4041

encapsulated complexes and the mean particle size as obtained from TEM. Multiplication with the per complex extinction coefficient (40 000 $M^{-1}$ $cm^{-1}$ at 350 nm) and the QY then yields the brightness

$$B = N \varepsilon QY$$

The fluorescence cross section, in $cm^2$, can be obtained by multiplying this value with $3.82 \times 10^{-21}$.

*Immobilization of ECP-NPs.* The surface of CELLview Petri dishes was treated overnight with 1 M NaOH. Then, the Petri dish surface was extensively rinsed with ultrapure water and incubated with PEI solution (2 mg $mL^{-1}$ in 20 mM tris-buffer at pH 7.4, 150 mM NaCl) at 37 °C for 1.5 h followed by rinsing with ultrapure water. Solutions of ECP-NPs in water at 40 $\mu$g $mL^{-1}$ were sonicated for 15 min and diluted in ultrapure water to 0.8 $\mu$g $mL^{-1}$ (for PMMA-$SO_3H$ 1%, 40% [Eu(tta)$_3$phen]) or 0.4 $\mu$g $mL^{-1}$ (for PMMA-COOH 10%, 40% [Eu(tta)$_3$phen]). Petri dishes were incubated with NPs for 2 h, rinsed, and immersed in ultrapure water. PMMA-$SO_3H$ 3% and 40% [Eu(tta)$_3$phen] NPs were also sonicated for 15 min and diluted to 2 $\mu$g $mL^{-1}$ in PVA at 15% in water and heated to 70 °C.

**Cell Culture.** Cells were grown in DMEM supplemented with 10% FBS, 1% penicillin/streptomycin, and 2 mM L-glutamine at 37 °C and 5% $CO_2$. The cells were passaged with trypsin−EDTA 0.05%.

*Cell Incubation with ECP-NPs.* HeLa cells were seeded at $3 \times 10^5$ cells/dish in Nunclon Delta Petri dishes and incubated at 37 °C and 5% $CO_2$ overnight. The following day, ECP-NPs were sonicated for 15 min and then mixed rapidly with Opti-MEM at 4 $\mu$g $mL^{-1}$. Cells were washed with HBSS and incubated with ECP-NPs in Opti-MEM for 3 h at 37 °C, followed by rinsing with phosphate-buffered saline. Cells were detached using trypsin and centrifuged for 5 min at 37 °C and 1500 rpm. Cells were resuspended and seeded at $5 \times 10^4$ cells/well in LabTek chambers previously coated with fibronectin at 10 $\mu$g $mL^{-1}$. Cells were incubated for 1 h and then imaged at 37 °C.

*Costaining with DiD and LysoTracker.* DiD was used for plasma membrane labeling of HeLa cells following 20 h of incubation with ECP-NPs. First, cells were suspended using trypsin in 1 mL of complete culture medium. Then, DiD in dimethylformamide was added at the final concentration of 5 $\mu$M and gently mixed. Cells were incubated for 10 min at 37 °C and 5% $CO_2$. To remove nonincorporated DiD, cells were washed three times using centrifugation at 1500 rpm and 37 °C for 5 min. After each spin, cells were resuspended in a fresh complete culture medium. For labeling of endosomes/lysosomes, HeLa cells were first incubated with ECP-NPs for 24 h and then coincubated with green LysoTracker in complete DMEM at 50 nM for 30 min. In both cases, cells were imaged in Opti-MEM.

**TG PL Microscopy.** Single NP imaging and cell imaging were performed using a wide-field, inverted microscope (Olympus IX71) that uses a UV laser (349 nm, 300 Hz, Nd:YLF, Triton, Spectra Physics) for pulsed excitation and an intensified CCD camera (ICCD, PI-MAX3, Princeton Instruments) for TG detection. Laser irradiance on the sample was 0.24 W $cm^{-2}$, which corresponds to a UV light dose of 1 $\mu$J $cm^{-2}$. The laser beam was redirected onto the sample with a 405 nm dichroic mirror (Di02-R405, Semrock Inc.). PL signals of ECP-NPs were collected with a high numerical aperture (NA = 1.35) immersion oil objective (UPLSAPO 60× O, Olympus) and detected using a 605 nm bandpass filter (FF01-605/15-25, Semrock Inc.). Acquisition settings in Winview software controlling the camera were fixed at a delay time of 10 $\mu$s, gatewidth of 0.6 ms, gates/exposure of 200 (for single NP imaging) or 100 (for cell imaging), and intensifier gain of 100 V. DIC images were acquired with no delay time, a gatewidth of 300 ms, gates/exposure of 1, accumulations of 10, and an intensifier gain at 6 V. The background acquired on a bare substrate with the same acquisition settings (gating sequence, laser frequency) was subtracted from the raw images. For single NP imaging, the mean intensities of circular regions of 6 pixels around the particles were measured for at least 200 particles and the background signal was subtracted. Zones with intensities above four times the mean per particle intensity were excluded from the analysis.

Details on steady-state and 3D imaging as well as on Photon counting can be found in the Supporting Information

## ■ ASSOCIATED CONTENT

### Supporting Information

The Supporting Information is available free of charge on the ACS Publications website at DOI: 10.1021/acs.chemmater.9b00576.

Additional experimental details, as well as TEM images, absorption and emission spectra, and micrographs of single NPs and cells incubated with ECP-NPs (PDF)

Scan through a cell after incubation with PMMA-COOH 10% NPs loaded with 40 wt % of [Eu(tta)$_3$phen] (AVI)

## ■ AUTHOR INFORMATION


### Corresponding Authors

*E-mail: niko.hildebrandt@u-psud.fr (N.H.).
*E-mail: reisch@unistra.fr (A.R.).

### ORCID

Aline M. Nonat: 0000-0003-0478-5039
Loïc J. Charbonnière: 0000-0003-0328-9842
Andrey S. Klymchenko: 0000-0002-2423-830X
Niko Hildebrandt: 0000-0001-8767-9623
Andreas Reisch: 0000-0003-1154-7637


### Author Contributions

‖M.C.D.S. and A.R. contributed equally to this work.

### Author Contributions

The manuscript was written through contributions of all authors. All authors have given approval to the final version of the manuscript.

### Notes

The authors declare no competing financial interest.

## ■ ACKNOWLEDGMENTS

The authors thank the French Agence National de la Recherche (ANR project "neutrinos", ANR JC/JC project "supertrack" 16-CE09-0007) and the European Commission (Horizon2020, FET-Open project "PROSEQO", ERC Consolidator Grant "BRIGHTSENS") for financial support and C. Ruhlmann and C. Crucifix from the FRISBI platform (ANR-10-INBS-05) for help with electron microscopy.

## ■ REFERENCES


(1) Wolfbeis, O. S. An Overview of Nanoparticles Commonly Used in Fluorescent Bioimaging. *Chem. Soc. Rev.* **2015**, *44*, 4743−4768.

(2) Howes, P. D.; Chandrawati, R.; Stevens, M. M. Colloidal Nanoparticles as Advanced Biological Sensors. *Science* **2014**, *346*, No. 1247390.

(3) Wegner, K. D.; Hildebrandt, N. Quantum Dots: Bright and Versatile in Vitro and in Vivo Fluorescence Imaging Biosensors. *Chem. Soc. Rev.* **2015**, *44*, 4792−4834.

(4) Zhou, J.; Yang, Y.; Zhang, C. Toward Biocompatible Semiconductor Quantum Dots: From Biosynthesis and Bioconjugation to Biomedical Application. *Chem. Rev.* **2015**, *115*, 11669−11717.

(5) Haase, M.; Schäfer, H. Upconverting Nanoparticles. *Angew. Chem., Int. Ed.* **2011**, *50*, 5808−5829.

(6) Gargas, D. J.; Chan, E. M.; Ostrowski, A. D.; Aloni, S.; Altoe, M. V. P.; Barnard, E. S.; Sanii, B.; Urban, J. J.; Milliron, D. J.; Cohen, B. E.; et al. Engineering Bright Sub-10-Nm Upconverting Nanocrystals for Single-Molecule Imaging. *Nat. Nanotechnol.* **2014**, *9*, 300−305.

(7) Ostrowski, A. D.; Chan, E. M.; Gargas, D. J.; Katz, E. M.; Han, G.; Schuck, P. J.; Milliron, D. J.; Cohen, B. E. Controlled Synthesis and Single-Particle Imaging of Bright, Sub-10 Nm Lanthanide-Doped Upconverting Nanocrystals. *ACS Nano* **2012**, *6*, 2686−2692.




DOI: 10.1021/acs.chemmater.9b00576
*Chem. Mater.* 2019, 31, 4034−4041

(8) Resch-Genger, U.; Gorris, H. H. Perspectives and Challenges of Photon-Upconversion Nanoparticles - Part I: Routes to Brighter Particles and Quantitative Spectroscopic Studies. *Anal. Bioanal. Chem.* **2017**, *409*, 5855−5874.
(9) Zheng, X. T.; Ananthanarayanan, A.; Luo, K. Q.; Chen, P. Glowing Graphene Quantum Dots and Carbon Dots: Properties, Syntheses, and Biological Applications. *Small* **2015**, *11*, 1620−1636.
(10) Kang, Z.; Liu, Y.; Gao, J.; Zhu, M. Carbon Dots for Environmental and Energy Applications: Advances, Challenges and Promises. *Inorg. Chem. Front.* **2017**, *4*, 1963−1986.
(11) Cardoso Dos Santos, M.; Goetz, J.; Bartenlian, H.; Wong, K.-L.; Charbonnière, L. J.; Hildebrandt, N. Autofluorescence-Free Live-Cell Imaging Using Terbium Nanoparticles. *Bioconjug. Chem.* **2018**, *29*, 1327−1334.
(12) Sy, M.; Nonat, A.; Hildebrandt, N.; Charbonnière, L. J. Lanthanide-Based Luminescence Biolabelling. *Chem. Commun.* **2016**, *52*, 5080−5095.
(13) Dong, H.; Du, S.-R.; Zheng, X.-Y.; Lyu, G.-M.; Sun, L.-D.; Li, L.-D.; Zhang, P.-Z.; Zhang, C.; Yan, C.-H. Lanthanide Nanoparticles: From Design toward Bioimaging and Therapy. *Chem. Rev.* **2015**, *115*, 10725−10815.
(14) Kaeser, A.; Schenning, A. P. H. J. Fluorescent Nanoparticles Based on Self-Assembled $\pi$-Conjugated Systems. *Adv. Mater.* **2010**, *22*, 2985−2997.
(15) Görl, D.; Zhang, X.; Würthner, F. Molecular Assemblies of Perylene Bisimide Dyes in Water. *Angew. Chem., Int. Ed.* **2012**, *51*, 6328−6348.
(16) Li, K.; Liu, B. Polymer-Encapsulated Organic Nanoparticles for Fluorescence and Photoacoustic Imaging. *Chem. Soc. Rev.* **2014**, *43*, 6570−6597.
(17) Peng, H.-S.; Chiu, D. T. Soft Fluorescent Nanomaterials for Biological and Biomedical Imaging. *Chem. Soc. Rev.* **2014**, *44*, 4699−4722.
(18) Reisch, A.; Klymchenko, A. S. Fluorescent Polymer Nanoparticles Based on Dyes: Seeking Brighter Tools for Bioimaging. *Small* **2016**, *12*, 1968−1992.
(19) Mochalin, V. N.; Shenderova, O.; Ho, D.; Gogotsi, Y. The Properties and Applications of Nanodiamonds. *Nat. Nanotechnol.* **2012**, *7*, 11−23.
(20) Haziza, S.; Mohan, N.; Loe-Mie, Y.; Lepagnol-Bestel, A. M.; Massou, S.; Adam, M. P.; Le, X. L.; Viard, J.; Plancon, C.; Daudin, R.; et al. Fluorescent Nanodiamond Tracking Reveals Intraneuronal Transport Abnormalities Induced by Brain-Disease-Related Genetic Risk Factors. *Nat. Nanotechnol.* **2017**, *12*, 322−328.
(21) Croce, A. C.; Bottiroli, G. Autofluorescence Spectroscopy and Imaging: A Tool for Biomedical Research and Diagnosis. *Eur. J. Histochem.* **2014**, *58*, No. 2461.
(22) Kusumi, A.; Tsunoyama, T. A.; Hirosawa, K. M.; Kasai, R. S.; Fujiwara, T. K. Tracking Single Molecules at Work in Living Cells. *Nat. Chem. Biol.* **2014**, *10*, 524−532.
(23) Shen, H.; Tauzin, L. J.; Baiyasi, R.; Wang, W.; Moringo, N.; Shuang, B.; Landes, C. F. Single Particle Tracking: From Theory to Biophysical Applications. *Chem. Rev.* **2017**, *117*, 7331−7376.
(24) Tang, S.; Moayeri, M.; Chen, Z.; Harma, H.; Zhao, J.; Hu, H.; Purcell, R. H.; Leppla, S. H.; Hewlett, I. K. Detection of Anthrax Toxin by an Ultrasensitive Immunoassay Using Europium Nanoparticles. *Clin. Vaccine Immunol.* **2009**, *16*, 408−413.
(25) Tan, W.; Wang, K.; He, X.; Zhao, X. J.; Drake, T.; Wang, L.; Bagwe, R. P. Bionanotechnology Based on Silica Nanoparticles. *Med. Res. Rev.* **2004**, *24*, 621−638.
(26) Härmä, H.; Soukka, T.; Lövgren, T. Europium Nanoparticles and Time-Resolved Fluorescence for Ultrasensitive Detection of Prostate-Specific Antigen. *Clin. Chem.* **2001**, *47*, 561−568.
(27) Davies, A.; Lewis, D. J.; Watson, S. P.; Thomas, S. G.; Pikramenou, Z. PH-Controlled Delivery of Luminescent Europium Coated Nanoparticles into Platelets. *Proc. Natl. Acad. Sci. U.S.A.* **2012**, *109*, 1862−1867.
(28) Wong, K. L.; Law, G. L.; Murphy, M. B.; Tanner, P. A.; Wong, W. T.; Lam, P. K. S.; Lam, M. H. W. Functionalized Europium Nanorods for in Vitro Imaging. *Inorg. Chem.* **2008**, *47*, 5190−5196.
(29) Di, W.; Li, J.; Shirahata, N.; Sakka, Y.; Willinger, M.; Pinna, N. Photoluminescence, Cytotoxicity and in Vitro Imaging of Hexagonal Terbium Phosphate Nanoparticles Doped with Europium. *Nanoscale* **2011**, *3*, 1263−1269.
(30) Manning, H. C.; Goebel, T.; Thompson, R. C.; Price, R. R.; Lee, H.; Bornhop, D. J. Targeted Molecular Imaging Agents for Cellular-Scale Bimodal Imaging. *Bioconjug. Chem.* **2004**, *15*, 1488−1495.
(31) Väisänen, V.; Härmä, H.; Lilja, H.; Bjartell, A. Time-Resolved Fluorescence Imaging for Quantitative Histochemistry Using Lanthanide Chelates in Nanoparticles and Conjugated to Monoclonal Antibodies. *Luminescence* **2000**, *15*, 389−397.
(32) Kattel, K.; Park, J. Y.; Xu, W.; Kim, H. G.; Lee, E. J.; Bony, B. A.; Heo, W. C.; Chang, Y.; Kim, T. J.; Do, J. Y.; et al. Water-Soluble Ultrasmall Eu2O3 Nanoparticles as a Fluorescent Imaging Agent: In Vitro and in Vivo Studies. *Colloids Surf., A* **2012**, *394*, 85−91.
(33) Beaurepaire, E.; Buissette, V.; Sauviat, M. P.; Giaume, D.; Lahlil, K.; Mercuri, A.; Casanova, D.; Huignard, A.; Martin, J. L.; Gacoin, T.; et al. Functionalized Fluorescent Oxide Nanoparticles: Artificial Toxins for Sodium Channel Targeting and Imaging at the Single-Molecule Level. *Nano Lett.* **2004**, *4*, 2079−2083.
(34) Wu, S.; Han, G.; Milliron, D. J.; Aloni, S.; Altoe, V.; Talapin, D. V.; Cohen, B. E. Non-Blinking and Photostable Upconverted Luminescence from Single Lanthanide- Doped Nanocrystals. *Proc. Natl. Acad. Sci. U.S.A.* **2009**, *106*, 1−5.
(35) Zhang, J.; Ray, K.; Fu, Y.; Lakowicz, J. R. First Observation to Enhanced Luminescence from Single Lanthanide Chelate on Silver Nanorod. *Chem. Commun.* **2014**, *50*, 9383−9386.
(36) Laissue, P. P.; Alghamdi, R. A.; Tomancak, P.; Reynaud, E. G.; Shroff, H. Assessing Phototoxicity in Live Fluorescence Imaging. *Nat. Methods* **2017**, *14*, 657−661.
(37) Trofymchuk, K.; Reisch, A.; Didier, P.; Fras, F.; Gilliot, P.; Mely, Y.; Klymchenko, A. S. Giant Light-Harvesting Nanoantenna for Single-Molecule Detection in Ambient Light. *Nat. Photonics* **2017**, *11*, No. 657.
(38) Robin, M. P.; O'Reilly, R. K. Strategies for Preparing Fluorescently Labelled Polymer Nanoparticles. *Polym. Int.* **2015**, *64*, 174−182.
(39) Robin, M. P.; Raymond, J. E.; O'Reilly, R. K. One-Pot Synthesis of Super-Bright Fluorescent Nanogel Contrast Agents Containing a Dithiomaleimide Fluorophore. *Mater. Horiz.* **2014**, *2*, 54−59.
(40) Reisch, A.; Didier, P.; Richert, L.; Oncul, S.; Arntz, Y.; Mély, Y.; Klymchenko, A. S. Collective Fluorescence Switching of Counterion-Assembled Dyes in Polymer Nanoparticles. *Nat. Commun.* **2014**, *5*, No. 4089.
(41) Reisch, A.; Trofymchuk, K.; Runser, A.; Fleith, G.; Rawiso, M.; Klymchenko, A. S. Tailoring Fluorescence Brightness and Switching of Nanoparticles through Dye Organization in the Polymer Matrix. *ACS Appl. Mater. Interfaces* **2017**, *9*, 43030−43042.
(42) Qin, W.; Li, K.; Feng, G.; Li, M.; Yang, Z.; Liu, B.; Tang, B. Z. Bright and Photostable Organic Fluorescent Dots with Aggregation-Induced Emission Characteristics for Noninvasive Long-Term Cell Imaging. *Adv. Funct. Mater.* **2014**, *24*, 635−643.
(43) Binnemans, K. Lanthanide-Based Luminescent Hybrid Materials. *Chem. Rev.* **2009**, *109*, 4283−4374.
(44) Feng, J.; Zhang, H. Hybrid Materials Based on Lanthanide Organic Complexes: A Review. *Chem. Soc. Rev.* **2012**, *42*, 387−410.
(45) Desbiens, J.; Bergeron, B.; Patry, M.; Ritcey, A. M. Polystyrene Nanoparticles Doped with a Luminescent Europium Complex. *J. Colloid Interface Sci.* **2012**, *376*, 12−19.
(46) Bai, G.; Tsang, M.-K.; Hao, J. Luminescent Ions in Advanced Composite Materials for Multifunctional Applications. *Adv. Funct. Mater.* **2016**, *26*, 6330−635.
(47) Sun, W.; Yu, J.; Deng, R.; Rong, Y.; Fujimoto, B.; Wu, C.; Zhang, H.; Chiu, D. T. Semiconducting Polymer Dots Doped with Europium Complexes Showing Ultranarrow Emission and Long


DOI: 10.1021/acs.chemmater.9b00576
*Chem. Mater.* 2019, 31, 4034−4041

Luminescence Lifetime for Time-Gated Cellular Imaging. *Angew. Chem., Int. Ed.* **2013**, *52*, 11294−11297.
(48) Li, Q.; Zhang, J.; Sun, W.; Yu, J.; Wu, C.; Qin, W.; Chiu, D. T. Europium-Complex-Grafted Polymer Dots for Amplified Quenching and Cellular Imaging Applications. *Langmuir* **2014**, *30*, 8607−8614.
(49) Peng, H.; Stich, M. I. J.; Yu, J.; Sun, L.; Fischer, L. H.; Wolfbeis, O. S. Luminescent Europium(III) Nanoparticles for Sensing and Imaging of Temperature in the Physiological Range. *Adv. Mater.* **2010**, *22*, 716−719.
(50) Huhtinen, P.; Kivelä, M.; Kuronen, O.; Hagren, V.; Takalo, H.; Tenhu, H.; Lövgren, T.; Härmä, H. Synthesis, Characterization, and Application of Eu(III), Tb(III), Sm(III), and Dy(III) Lanthanide Chelate Nanoparticle Labels. *Anal. Chem.* **2005**, *77*, 2643−2648.
(51) Wartenberg, N.; Raccurt, O.; Imbert, D.; Mazzanti, M.; Bourgeat-Lami, E. Luminescent Latex Particles Loaded with Anionic Lanthanide Complexes: A Versatile Platform for Multicolour Optical Coding. *J. Mater. Chem. C* **2013**, *1*, 2061−2068.
(52) Pihlasalo, S.; Mariani, L.; Härmä, H. Quantitative and Discriminative Analysis of Nucleic Acid Samples Using Luminometric Nonspecific Nanoparticle Methods. *Nanoscale* **2016**, *8*, 5902−5911.
(53) Takei, Y.; Arai, S.; Murata, A.; Takabayashi, M.; Oyama, K.; Ishiwata, S.; Takeoka, S.; Suzuki, M. A Nanoparticle-Based Ratiometric and Self-Calibrated Fluorescent Thermometer for Single Living Cells. *ACS Nano* **2014**, *8*, 198−206.
(54) Hildebrandt, N.; Wegner, K. D.; Algar, W. R. Luminescent Terbium Complexes: Superior Förster Resonance Energy Transfer Donors for Flexible and Sensitive Multiplexed Biosensing. *Coord. Chem. Rev.* **2014**, *273*−*274*, 125−138.
(55) Reisch, A.; Runser, A.; Arntz, Y.; Mély, Y.; Klymchenko, A. S. Charge-Controlled Nanoprecipitation as a Modular Approach to Ultrasmall Polymer Nanocarriers: Making Bright and Stable Nanoparticles. *ACS Nano* **2015**, *9*, 5104−5116.
(56) Reisch, A.; Heimburger, D.; Ernst, P.; Runser, A.; Didier, P.; Dujardin, D.; Klymchenko, A. S. Protein-Sized Dye-Loaded Polymer Nanoparticles for Free Particle Diffusion in Cytosol. *Adv. Funct. Mater.* **2018**, *28*, No. 1805157.
(57) Stanimirov, S. S.; Hadjichristov, G. B.; Petkov, I. K. Emission Efficiency of Diamine Derivatives of Tris[4,4,4-Trifluoro-1-(2-Thienyl)-1,3-Butanediono]Europium. *Spectrochim. Acta, Part A* **2007**, *67*, 1326−1332.
(58) Etoc, F.; Balloul, E.; Vicario, C.; Normanno, D.; Liße, D.; Sittner, A.; Piehler, J.; Dahan, M.; Coppey, M. Non-Specific Interactions Govern Cytosolic Diffusion of Nanosized Objects in Mammalian Cells. *Nat. Mater.* **2018**, *17*, 740−746.
(59) Eliseeva, S. V.; Bünzli, J.-C. G. Lanthanide Luminescence for Functional Materials and Bio-Sciences. *Chem. Soc. Rev.* **2009**, *39*, 189−227.
(60) Fix, T.; Nonat, A.; Imbert, D.; Di Pietro, S.; Mazzanti, M.; Slaoui, A.; Charbonnière, L. J. Enhancement of Silicon Solar Cells by Downshifting with Eu and Tb Coordination Complexes. *Prog. Photovoltaics* **2016**, *24*, 1251−1260.
(61) Cardoso Dos Santos, M.; Hildebrandt, N. Recent Developments in Lanthanide-to-Quantum Dot FRET Using Time-Gated Fluorescence Detection and Photon Upconversion. *TrAC, Trends Anal. Chem.* **2016**, *84*, 60−71.
(62) Zhang, K. Y.; Yu, Q.; Wei, H.; Liu, S.; Zhao, Q.; Huang, W. Long-Lived Emissive Probes for Time-Resolved Photoluminescence Bioimaging and Biosensing. *Chem. Rev.* **2018**, *118*, 1770−1839.
(63) Weibel, N.; Charbonnière, L. J.; Guardigli, M.; Roda, A.; Ziessel, R. Engineering of Highly Luminescent Lanthanide Tags Suitable for Protein Labeling and Time-Resolved Luminescence Imaging. *J. Am. Chem. Soc.* **2004**, *126*, 4888−4896.



DOI: 10.1021/acs.chemmater.9b00576
*Chem. Mater.* 2019, 31, 4034−4041